Investigating the Catalytic Requirements of Perovskite Fuel Electrodes Using Ultra-Low Metal Loadings

Julian M. Paige[1], Duytam Vu[1], Tianyu Cao[1], Steven McIntosh[2], Raymond J. Gorte[1], and John M. Vohs[1]

[1] Department of Chemical and Biomolecular Engineering
University of Pennsylvania
Philadelphia, PA 19104, USA
[2] Department of Chemical and Biomolecular Engineering
Lehigh University
Bethlehem, PA 18015, USA
*Corresponding author: vohs@seas.upenn.edu

Abstract

Solid Oxide Fuel Cells (SOFC) with $La_{0.3}Sr_{0.7}TiO_3$ (LST)–yttria-stabilized ZrO_2 (YSZ) anodes were prepared by impregnation of LST into porous YSZ scaffolds and then modified by Atomic Layer Deposition (ALD) of Ni, Pt, Pd, Fe, Co. and CeO_2. Weight loadings as low as 0.01% of Pt, Ni, and Pd were sufficient to decrease anode impedances by orders of magnitude for operation in humidified H_2 at 973 K. The effects of CeO_2, Co, and Fe were less but still significant. Sintering at higher temperatures was important. Possible ways of stabilizing the metal particles and implications for developing ceramic anodes are discussed.

Keywords: Solid Oxide Fuel Cell, Atomic Layer Deposition, Electrocatalysis, Perovskite, Low Energy Ion Scattering

Introduction

Solid Oxide Electrochemical Cells (SOCs) are promising energy conversion devices that can be used to produce energy in fuel cell mode (SOFC) or, alternatively, to produce green hydrogen and carbon monoxide through electrolysis (SOEC) of water or carbon dioxide.[1] State of the art Ni-cermet fuel electrodes can exhibit good performance in both SOFC and SOEC modes; however, they also have several drawbacks including poor redox stability,[2,3] vulnerability to poisoning by sulfur,[4,5] and high catalytic activity for the formation of carbon fibers when exposed to CO, CO_2 or hydrocarbon-based fuels.[6,7] To overcome these shortcomings of Ni cermets, alternative fuel electrodes based on electronically conductive ceramics have been developed.[8–14] Several promising candidates for ceramic fuel electrodes include members of the perovskite (ABO_3) family: $La_{0.3}Sr_{0.7}TiO_3$ (LST),[15,16] $La_{0.8}Sr_{0.2}Cr_{0.5}Mn_{0.5}O_3$ (LSCM),[17–19] and $La_{0.8}Sr_{0.2}VO_3$ (LSV).[20] These materials are of interest because they are inert towards carbon formation, have high sulfur tolerance, and are redox stable. While the electronic conductivity of these perovskite electrodes is adequate, their catalytic activity is very poor. Therefore, much effort has been directed at enhancing their inherently poor catalytic activity by incorporating metal catalysts onto the electrode surface.

To take advantage of the potential sulfur and carbon tolerance of ceramic anodes, the catalyst must also be stable and precious metals are an excellent candidate for this application.[21] Because of the price, it is essential that metal loadings be very low when using these. Unfortunately, it is difficult to add very small amounts of precious metals to the ceramic composite and still achieve effective catalytic properties. The most common way to add catalyst is through wet infiltration with metal salts.[15-20] The amount of catalytic metal that is added is usually significant, at least 1 wt%. Another approach for providing catalytic activity to ceramic

anodes involves doping the B-site of the perovskite with a small amount of a reducible metal (Fe, Co, Ni, Pd, Pt, etc). Under reducing conditions, the metal can exsolve from the perovskite lattice and form metal particles that migrate to the surface.[22,23] Although exsolution catalysts have desirable properties, such as high catalytic activity, coking resistance, redox stability, and sintering resistance,[24] most of the catalytic metal is wasted because it remains trapped in the bulk.[25]

While some recent studies have investigated the performance of anodes with very low catalyst loadings,[26,27] there has yet to be a study that systematically investigates the minimum catalyst loading needed in order to achieve modest activity, and do so for a number of different materials. In the current study, Atomic Layer Deposition (ALD) was used to determine the minimum amount of metal catalyst required to achieve activity on par with that of Ni-YSZ (Ni Yttria-stabilized Zirconia) cermets using a ceramic anode composed of an LST-YSZ composite. In particular, we investigated the activity of the LST-YSZ||YSZ||LSF-YSZ cell before and after the addition of sub-monolayer amounts of transition metals (Fe, Ni, and Co), precious metals (Pt and Pd), or CeO_2. Herein, we will demonstrate that fuel electrodes modified with ultra-low catalysts loadings (~ 0.01 wt %) via ALD exhibit good performance in fuel cell mode using conventional materials in the electrolyte and oxygen electrode.

Experimental

SOFCs with a $La_{0.3}Sr_{0.7}TiO_3$-YSZ (LST-YSZ) anode and a $La_{0.8}Sr_{0.2}FeO_3$-YSZ (LSF-YSZ) cathode were prepared by infiltration of metal precursors into porous, YSZ scaffolds that were prepared in a manner similar to that described in detail in previous work.[16,28] The starting porous-dense-porous, YSZ wafers were fabricated by tape casting, using pore formers to achieve porosity in the outer layers. The 8 mol % yttria YSZ was purchased from TOSOH Corp. Further

details about the tape-casting process and the full list of ingredients used can be found elsewhere.[29] After calcination at 1673 K for 4 hours, the dense electrolyte was 1-cm in diameter and ~80-μm thick, while the 65% porous layers were 0.67-cm in diameter and ~50-60 μm thick. The electrode active area was 0.35 cm^2. Roughly 12 infiltration steps of the appropriate precursor solution ($La(NO_3)_3 \cdot 6H_2O$ (Alfa Aesar, 99.9%), $Sr(NO_3)_2$ (Alfa Aesar, 99%), and dihydroxy-bis (ammonium lactato) Ti(IV) 50 wt% solution (Alfa Aesar) or $Fe(NO_3)_3 \cdot 6H_2O$ (Fisher Scientific, 98.4%)) were required to give the proper loading of each perovskite (45 wt% LST, 35 wt% LSF). The molar ratios of the metals were 0.8-La:0.2-Sr:1-Fe for LSF, and 0.3-La:0.7-Sr:1-Ti for LST. LST was infiltrated first, and the cell was calcined to 1373 K for 4 hours. LSF was infiltrated next and the cell was calcined to 1123 K for 1.5 hours. Two cells had either Ni or Pt infiltrated into the LST-YSZ electrode using a $Ni(NO_3)_2 \cdot 6H_2O$ solution or $Pt(NH_4)_4(NO_3)_2$ solution, respectively.

ALD modification of the pristine LST-YSZ||YSZ||LSF-YSZ cells was performed in a homebuilt apparatus, using procedures that have been described in detail in other publications.[30,31] Most commercial ALD systems use a short pulse of the precursor vapor in a carrier gas during growth. While this works well for planar samples, diffusional limitations encountered for highly porous samples can result in growth primarily on the external surface using this approach.[31] To overcome this limitation without using a carrier gas in a flow configuration, we evacuated the sample to a pressure of ~ 200 millitorr and then exposed it to the vapor of the ALD precursor for ~ 5 min. Removal of excess precursor was achieved by 5 min of evacuation. The exposure and evacuation temperatures were 473 K for the Co, Ni, and Pt precursors, and 453 K for the Pd precursor. The Ce precursor was deposited at 503 K and the Fe precursor was deposited at 523 K. The samples were removed from the system and oxidized in

air at 773 K for 5 min for the oxidation part of each ALD cycle. This process was repeated for the desired number of cycles. The precursors used in this study were: $Pd(TMHD)_2$ ($5.6\cdot10^{13}$ Pd atoms$\cdot$cm$^{-2}\cdot$cycle^{-1}), $Co(TMHD)_3$ ($7.0\cdot10^{13}$ Co atoms$\cdot$cm$^{-2}\cdot$cycle^{-1}), $Ce(TMHD)_4$ ($3.8\cdot10^{13}$ Ce atoms$\cdot$cm$^{-2}\cdot$cycle^{-1}), and $Ni(TMHD)_2$ ($9.0\cdot10^{13}$ Ni atoms$\cdot$cm$^{-2}\cdot$cycle^{-}), (where TMHD=2,2,6,6-tetramethyl-3,5-heptanedionato). Ferrocene ($1.0\cdot10^{14}$ Fe atoms$\cdot$cm$^{-2}\cdot$cycle^{-1}), and Pt(II)acetylacetonate (Pt-acac) ($1.0\cdot10^{14}$ atoms$\cdot$cm$^{-2}\cdot$cycle^{-1}), all of which were purchased from Strem Chemical Inc. Growth rates were determined gravimetrically using high surface area γ-Al_2O_3 powders as the substrate in order to enhance the accuracy of the measurement. Note that we have shown previously that ALD growth rates are similar on various metal-oxide substrates.[32,33] Cells modified with ALD will be denoted by the number of ALD cycles and material deposited. *e.g.* 1 Ni ALD. Cells where the LST-YSZ electrode was infiltrated with Ni or Pt will be denoted as Inf Ni and Inf Pt. Table 1 shows the metal loadings on the LST-YSZ electrodes modified by ALD or infiltration that were used in this study.

X-ray Diffraction (XRD) was used to confirm the formation of the correct perovskite phases in the electrodes (Figure 1a) and was performed with a Rigaku Miniflex diffractogram with a CuKα X-ray source (λ=0.15416 nm). Scanning Electron Microscopy (SEM) was performed with a FEI Quanta 600 FEG ESEM under 0.15 torr of humidity. High Sensitivity-Low Energy Ion Scattering spectroscopy (HS-LEIS) was used to determine the coverage of the ALD-deposited metals and were acquired using a Qtac 100 HS-LEIS spectrometer system using a 5 keV Ne^+ beam ($1\cdot10^{14}$ ions$\cdot$cm^{-2}). Prior to LEIS analysis the samples were lightly sputtered with a 0.5 keV Ar^+ beam ($7\cdot10^{14}$ ions$\cdot$cm^{-2}) beam until the surface adventitious carbon signal was eliminated. Brunauer-Emmett-Teller (BET) surface areas were measured using LST-YSZ slabs (0.31 m$^2\cdot$g^{-1}) that were made from the same porous tapes that were used to construct the

electrochemical cells using Kr at 78 K as the adsorbent. Electrode porosity was determined by measuring the mass of water required to fill the pores and was typically near 65 %. The scaffold weight was determined using its thickness, porosity and the bulk density of YSZ.

The electrochemical performance of the cells was measured using a Gamry Instruments impedance spectrometer/potentiostat. For cell performance testing a gas containing 90% H_2 and 10% H_2O was fed to the LST-YSZ anode at a flowrate of 40 ml/min, and the LSF-YSZ electrode was exposed to air. Electrochemical Impedance Spectroscopy (EIS) was performed with a 1-mA AC perturbation at open circuit, from 300 kHz to 0.1 Hz. IV-curves were measured by sweeping the voltage from 1.5 V to 0 V at a scanning rate of 0.01 $V \cdot s^{-1}$ and a 10 Hz acquisition rate. Ag wires and Ag paste, which have minimal catalytic activity, were used as current collectors. The cell was sealed to an alumina tube using Aremco Cermabond 552. The seal was cured at 503 K for 2 hours before ramping at 2 $K \cdot min^{-1}$ in N_2/H_2 to 873K for testing. Cells were ramped from 873 K to 1123 K at 2 $K \cdot min^{-1}$, with cell testing every 50 K after the temperature stabilized. Cells were held at 1123 K for 15 mins.

Results

To characterize the effect of catalyst addition to the LST-YSZ anodes, we prepared a base case LST-YSZ||YSZ||LSF-YSZ cell, as shown in Figure 1. XRD patterns for a bare YSZ scaffold and one infiltrated with LST are given in Figure 1a. These demonstrate that the infiltration and annealing procedure produced the desired LST perovskite phase with no evidence for the presence of any binary oxides. Figure 1b is a low-resolution, cross-sectional image of an LST-YSZ||YSZ||LSF-YSZ cell, showing that the scaffold layers adhere well to the electrolyte. Figures 1c and 1d display SEM images at higher resolution of the bare YSZ scaffold and the

LST-YSZ electrode with 5 ALD cycles of Pt addition near the electrolyte interface. A comparison of the two demonstrates that the LST, which corresponds to the rough features on the otherwise smooth surface of the YSZ, is uniformly distributed to the electrolyte interface. Pt is not visible in these images.

HS-LEIS was used to confirm that the metal coverages on the cell were consistent with the ALD growth rates measured gravimetrically on the high-surface-area substrates. HS-LEIS spectra for an LST-YSZ electrode before and after Pt addition and before reduction are shown in Figure 2. The spectrum for the pristine LST-YSZ electrode contains peaks at 963 eV, 2218 eV and 3005 eV which correspond to Ti, Sr, and La, respectively. Zr and Y may also contribute to the Sr peak at 2218 eV due to their similar atomic masses; however, our previous studies with infiltrated ceramic electrodes indicate that the infiltration process usually produces an oxide film that completely covers the exposed surface of the YSZ scaffold.[16,28]

The spectra of the Pt-containing samples were obtained after deposition by ALD and calcination in air at 773 K. Although the HS-LEIS spectrum obtained after 1 Pt ALD cycle is similar to that of the pristine sample, a small Pt peak centered at 3519 eV is resolvable, as shown in the inset. Since 1 ALD cycle is predicted to add only $1 \cdot 10^{14}$ Pt/cm^2, a coverage that is 10% of the surface atoms on a Pt(111) surface, the HS-LEIS result is roughly consistent with the ALD growth rates, especially considering that Pt likely forms particles after calcination to remove the precursor ligands.[34] After 5 Pt ALD cycles ($5 \cdot 10^{14}$ Pt/cm^2, equivalent to 0.5 monolayer), the Pt peak is much more prominent. The relatively small change in the intensity of other peaks in the spectrum demonstrates that the Pt covers only a fraction of the surface, suggesting again that the Pt has formed particles.

Analogous HS-LEIS data for a pristine electrode and ones modified with 1 ($0.9 \cdot 10^{14}$ Ni/cm^2) and 5 ($4.5 \cdot 10^{14}$ Ni/cm^2) Ni ALD cycles are displayed in Figure 3. In these data, the Ni peak appears at 1324 eV. An exact comparison of Ni and Pt intensities is difficult because the sensitivities of the two elements are different; however, the intensity of the Ni peak after 1 ALD cycle is clearly higher than that obtained for Pt after 1 cycle, even though the sensitivity should be higher for Pt because of its larger atomic mass. There was also a small decrease in the intensities of the substrate peaks after 5 ALD cycles. Since Ni will likely only form particles after reduction, the results here suggest Ni forms a more uniform film.

The effect on electrode performance of adding Pd catalysts by impregnation to LST-YSZ composites has previously reported to be very large due to the catalytic properties of Pd.[16,17] To demonstrate that Ni and Pt can lead to similar enhancements, we prepared cells with 1-wt% Ni or 0.5-wt% Pt added by impregnation into the LST-YSZ composite electrodes. V-I polarization curves and open-circuit impedance spectra for the pristine, Ni-infiltrated, and Pt-infiltrated LST-YSZ||YSZ||LSF-YSZ cells, measured at 973 K, are shown in Figures 4a and 4b. In agreement with previous reports, the performance of the unmodified LST-YSZ||YSZ||LSF-YSZ cell was very poor. Although the open-circuit potential was greater than 1.0 V in humidified H_2 and the ohmic resistance of the cell was less than 0.5 $\Omega \cdot cm^2$, a value consistent with the 80-μm thick YSZ electrolyte,[35] the maximum power density was only 13 $mW \cdot cm^{-2}$ due to the very large non-ohmic, cell impedance. The addition of Pt (0.5 wt %) or Ni (1 wt%) did not change the ohmic resistance of the cell but dramatically decreased the non-ohmic component to approximately 0.5 $\Omega \cdot cm^2$ in the case of Pt and 1.0 $\Omega \cdot cm^2$ in the case of Ni. Since the non-ohmic losses include an estimated 0.15 $\Omega \cdot cm^2$ from the LSF-YSZ cathode,[28] the anode performance after adding Pt or Ni is reasonably good.

The metal content after 1 or 5 ALD cycles of Pt or Ni can be determined from the growth rates and the surface area of the LST-YSZ electrode, which was measured to be 0.31 m^2/g. For Pt, the weight loadings corresponding to 1 and 5 ALD cycles were 0.01 and 0.05-wt%, respectively ($1 \cdot 10^{14}$ Pt/cm^2 and $5 \cdot 10^{14}$ Pt/cm^2 respectively). Polarization curves and impedance spectra at 973 K for the 1 Pt ALD and 5 Pt ALD cells are displayed in Figure 5a and 5b, respectively (Performance data at additional temperatures are in Figure S1a). Data for the pristine and Inf Pt cells are also included in the figure for comparison. These data show that 1 Pt ALD cycle is sufficient to dramatically improve the electrode performance, with the R_p decreasing to 1.86 $\Omega \cdot cm^2$ and the maximum power density increasing to 120 $mW \cdot cm^{-2}$. After 5 Pt ALD cycles, the performance was nearly the same as that of the Inf Pt cell. The 5 Pt ALD cell has an R_p of 0.54 $\Omega \cdot cm^2$ and a maximum power density of 250 $mW \cdot cm^{-2}$. With only 5 cycles of Pt ALD, the performance is now comparable to that of the Pt infiltrated cell. These results demonstrate that very small amounts of a catalytic metal are sufficient to achieve high performance.

Figure 6 displays analogous polarization curves and impedance data at 973 K for cells with Ni catalysts added by infiltration or ALD (performance data at additional temperatures are in Figure S1b). For comparison purposes, data for the pristine cell (no catalyst) are also included in the Figure 6a. The trends observed for Ni are similar to those for Pt, with a single Ni ALD cycle dramatically improving electrode performance and decreasing the R_p to 1.90 $\Omega \cdot cm^2$ and producing a maximum power density of 150 $mW \cdot cm^{-2}$. Additional increases in performance were observed when the number of Ni ALD cycles was increased to 5. Interestingly, the performance of the 5 Ni ALD cell surpassed that of the cell with infiltrated Ni, even though it had a Ni metal

weight loading of only 0.014%. The R_p and peak power density for the 5 Ni ALD cell were 0.77 $\Omega \cdot cm^2$ and 250 $mW \cdot cm^{-2}$ at 973 K.

The performance enhancements observed for LST/YSZ composite electrodes after addition of Ni or Pt via ALD demonstrate that, while an effective electrocatalyst is needed, the loading of the catalyst can be quite small and excellent performance can still be obtained if the dispersion is high. To investigate if similar levels of performance could be achieved using other catalysts, we also investigated the performance of cells in which the LST/YSZ composite electrode was modified by 5 ALD cycles of Pd, Fe, Co, or CeO_2. Polarization curves and impedance data at 973 K for these cells are presented in Figure 7 with data for additional temperatures reported in Figure S2. Not surprisingly based on the previous literature,[16,17] the 5 Pd ALD cell performed only slightly worse than the 5 Pt ALD and 5 Ni ALD cells, achieving a maximum power density of 190 $mW \cdot cm^{-2}$ and a R_p of 1.19 $\Omega \cdot cm^2$ at 973 K. The performance of the cell decorated with CeO_2 was also fairly good, achieving a maximum power density of 135 $mW \cdot cm^{-2}$ and a R_p of 1.27 $\Omega \cdot cm^2$ at 973 K. Reports from the literature also showed that CeO_2 is a reasonably effective anode catalyst, although all of that work was performed with much larger amounts of CeO_2.[18]

More surprising was the fact that the Co and Fe-modified electrodes exhibited relatively low performance, with the 5 Fe ALD and 5 Co ALD cells reaching maximum power densities of only 90 $mW \cdot cm^{-2}$ and 65 $mW \cdot cm^{-2}$, respectively, with polarization resistances of 1.97 $\Omega \cdot cm^2$ and 7.9 $\Omega \cdot cm^2$. Co, in particular, is a good hydrogenation catalyst and Co-based anodes have been shown to exhibit good performance.[36] Because Co could be incorporated into the perovskite lattice, it is possible that the small amounts of Co that were added to these cells enter the bulk LST phase. A similar possibility exists for Fe. In any case, the overall trend in the hydrogen

oxidation activity of the catalysts added to LST-YSZ electrodes using ALD is roughly as follows: Ni ≈ Pt ≈ Pd > CeO_2 > Fe > Co.

Finally, we investigated the thermal stability of the LST-YSZ electrodes that were modified by ALD of the metal catalysts. In these studies, the cell performance in humidified H_2 fuel was first measured at 973 K. Each cell was then heated to 1123 K and cooled back to 973 K, at which point the performance was again measured. The maximum power densities obtained for each cell before and after the high-temperature heat treatment are listed in Table 2. In all cases, the performance of the catalyst-containing cells decreased significantly after the heat treatment. Since the performance of the catalyst-free cell was not affected by the heat treatment, the changes in performance are not due to changes in the structure of the perovskite phase and must therefore be attributed to sintering of the catalysts.

Discussion

SOFC anodes must provide both electronic conductivity and catalytic activity for fuel oxidation. What we have shown in the present study is that miniscule amounts of catalytic metals like Pt and Ni are sufficient to provide good anode performance. This has important consequences for multiple reasons. First, the fact that such small amounts of catalyst are sufficient to achieve high performance in SOFC anodes implies that expensive metals, like Pt or Pd, could be used in practical applications. The advantage of using precious metals as the catalyst, rather than Ni, is that precious metals are much more resistant to coking and do not catalyze the formation of carbon filaments.[19] The use of coke-tolerant catalyst could allow SOFC to be operated on nearly dry methane. Obviously, stability of small metal particles at SOFC anode conditions is major issue, since maintaining dispersion at high temperatures can be very

difficult. There are indications that this is possible, however. Recent work with Pt on $LaFeO_3$ films demonstrated that high metal dispersions could be maintained, even after redox cycling at 1073 K.[37] In this previous work, High Angular Dark Field Scanning Transmission Electron Microscopy (STEM-HAADF) and Extended X-ray Absorption Fine Structure/ X-ray Absorption Near-Edge Structure (EXAFS/XANES) was used to investigate the sintering behavior of supported Pt catalysts prepared by ALD in the same manner as the current study. Pt ALD particles supported on ALD $LaFeO_3$ thin films remained quite small, roughly 1-2 nm spheres, after 1073 K treatment with multiple redox cycles.[37] However, Pt ALD particles supported on $MgAl_2O_4$ readily sintered to ~20 nm after the same treatment. The resulting images for $Pt/MgAl_2O_4$ is reproduced in Figure S3. In the current study, the metal particles are supported on essentially bulk metal-oxides (LST & YSZ), so it is expected that they would closely resemble that of the $Pt/MgAl_2O_4$ case which does not have strong metal-support interactions to stabilize the particles. The stability data presented in Table 2 supports this. In the future, it would be interesting to deposit thin film perovskites onto the surface of the electrode to stabilize the metal catalysts.

Second, the results obtained in this study further demonstrate that unintentional doping of ceramic anodes which can occur when catalytic metals are used as the current collector may significantly alter electrode performance. For example, two separate studies have shown that the performance of ceramic anodes could be dramatically improved when Pt is used as the current collector.[18,38] Although Pt that is spatially distant from the Three-Phase Boundary (TPB) sites near the electrolyte interface should not affect electrode performance, Pt is known to be highly mobile under oxidizing conditions due to the high vapor pressure of PtO_2.[39,40] It is likely that the improved performance observed in those two cases was due to Pt migration during cell

preparation. Pt migration will not be an issue with Ni-based electrodes since these are already catalytically active, but caution must be used in testing anodes of unknown catalytic activity.

The present results also suggest potential advantages for using ALD to incorporate catalytic components into SOFC anodes. Because the electrochemical reactions in SOFC anodes occur at TPB sites, electrode structure is critically important. As discussed by Tanner et al,[41] & Nicholas et al,[42] the best electrode performance is achieved when well-connected ion conducting channels of the electrolyte material are present within the electrode to carry ions from the electrolyte, far into the electrode. ALD provides an effective method for coating those channels with a catalytic metal, without adding unnecessary quantities.

The use of ALD in the fabrication of SOFC is still a relatively new area of research. The present study demonstrates that catalyst addition may be one important application.

Conclusions

We demonstrate that controlled amounts of catalytic materials, including Pt, Ni, Pd, CeO_2, Co, and Fe, can be incorporated into SOFC anodes by ALD. Ultralow loadings of Ni, Pt, or Pd, as low at 0.01-wt%, were found to be sufficient for achieving good electrode performance in conductive-ceramic anodes. Co, Fe, and CeO_2 were also found to enhance performance but to a lesser extent.

Acknowledgments

The authors would like to thank Dr. Ryan Thorpe of Lehigh's Institute for Functional Materials & Devices for performing the HS-LEIS characterization. This material is based upon work supported by the Department of Energy under Award Number DE-FE0031673. This report

Tables

Sample	wt % of metal in LST-YSZ electrode
1 Pt ALD	$1.0 \cdot 10^{-2}$
5 Pt ALD	$5.2 \cdot 10^{-2}$
1 Ni ALD	$2.7 \cdot 10^{-3}$
5 Ni ALD	$1.4 \cdot 10^{-2}$
5 Pd ALD	$1.5 \cdot 10^{-2}$
5 Co ALD	$1.2 \cdot 10^{-2}$
5 CeO_2 ALD	$1.7 \cdot 10^{-2}$
5 Fe ALD	$1.5 \cdot 10^{-2}$
Infiltrated Cells	
Inf Ni	1
Inf Pt	0.5

Table 1: Metal loadings in LST-YSZ electrode

Sample	Initial Power density (mW/cm^2)	After 1123 K (mW/cm^2)	% Change
Pristine	13	14	-
5 Co ALD	65	35	45
5 Fe ALD	90	50	46
1 Pt ALD	120	70	45
1 Ni ALD	150	85	43
5 Pd ALD	190	115	38
5 Pt ALD	250	135	46
5 Ni ALD	250	190	23

Table 2: Cell PPDs at 973 K before and after heat treatment

Figures

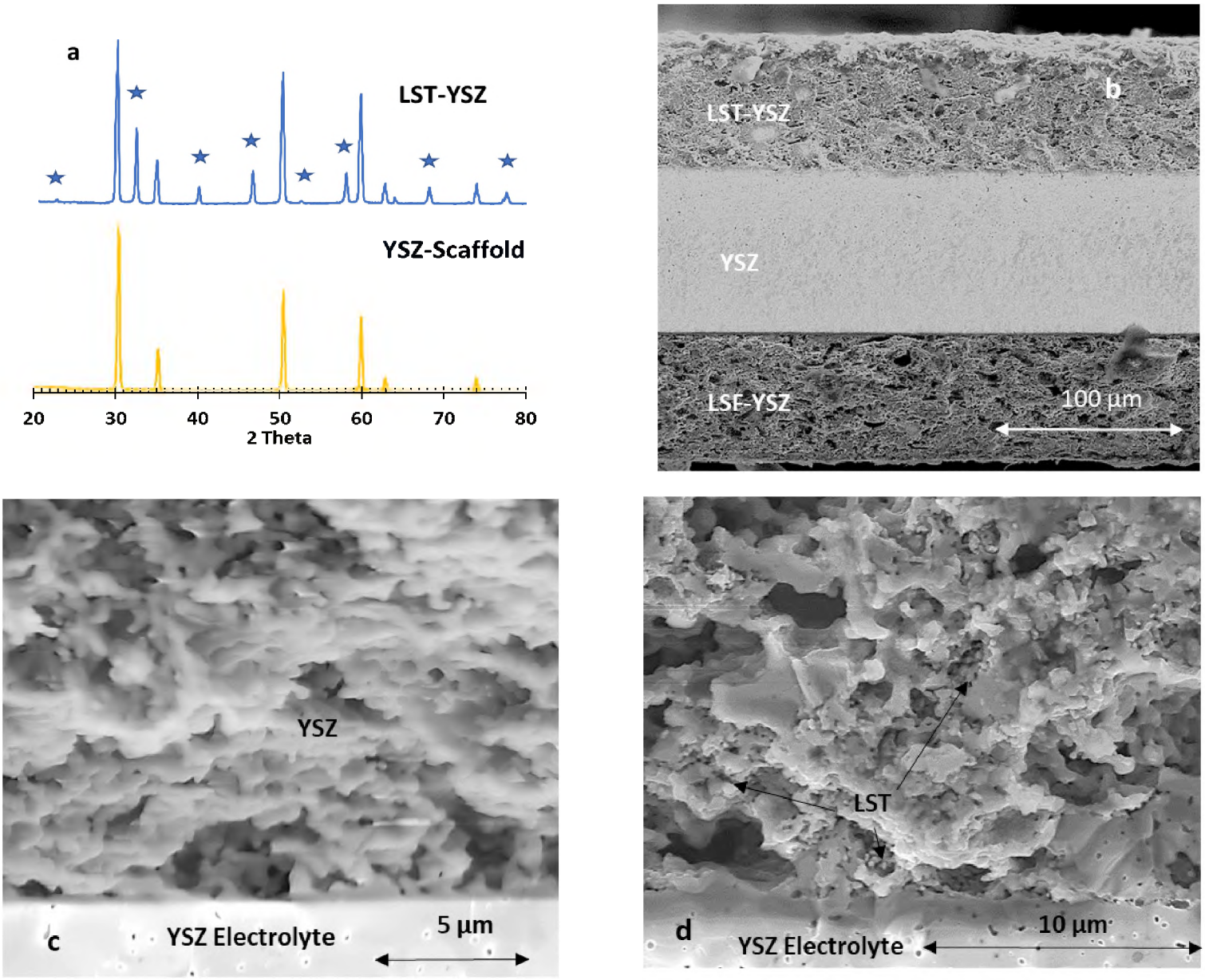

Figure 1. (a) XRD of YSZ and LST-YSZ scaffolds and (b-d) SEM images of YSZ and LST-YSZ scaffolds: (a) XRD pattern of the 45 wt% LST-YSZ composite and the bare YSZ scaffold (stars correspond to the perovskite peaks for the LST-YSZ composite), (b) cell cross section, (c) close-up of YSZ scaffold, (d) close up of the 5 Pt ALD LST-YSZ electrode.

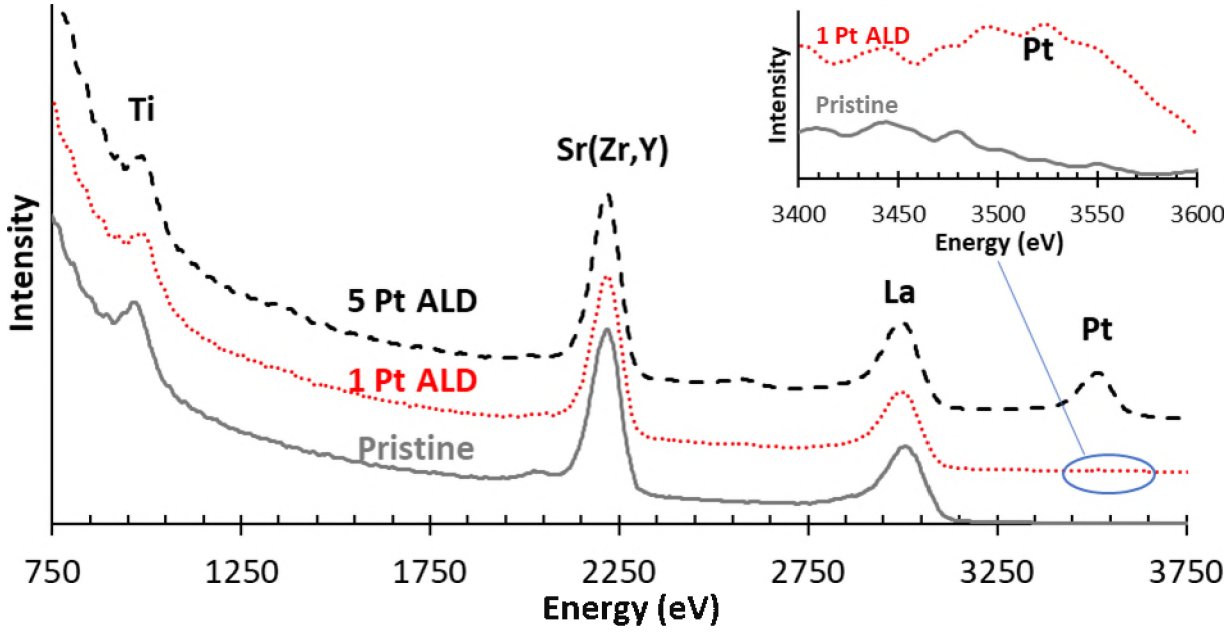

Figure 2. HS-LEIS spectra LST-YSZ electrodes with: 0, 1, or 5 cycles of Pt ALD. The ALD spectra are offset vertically for clarity. The inset highlights the small Pt signal on the 1 Pt ALD sample.

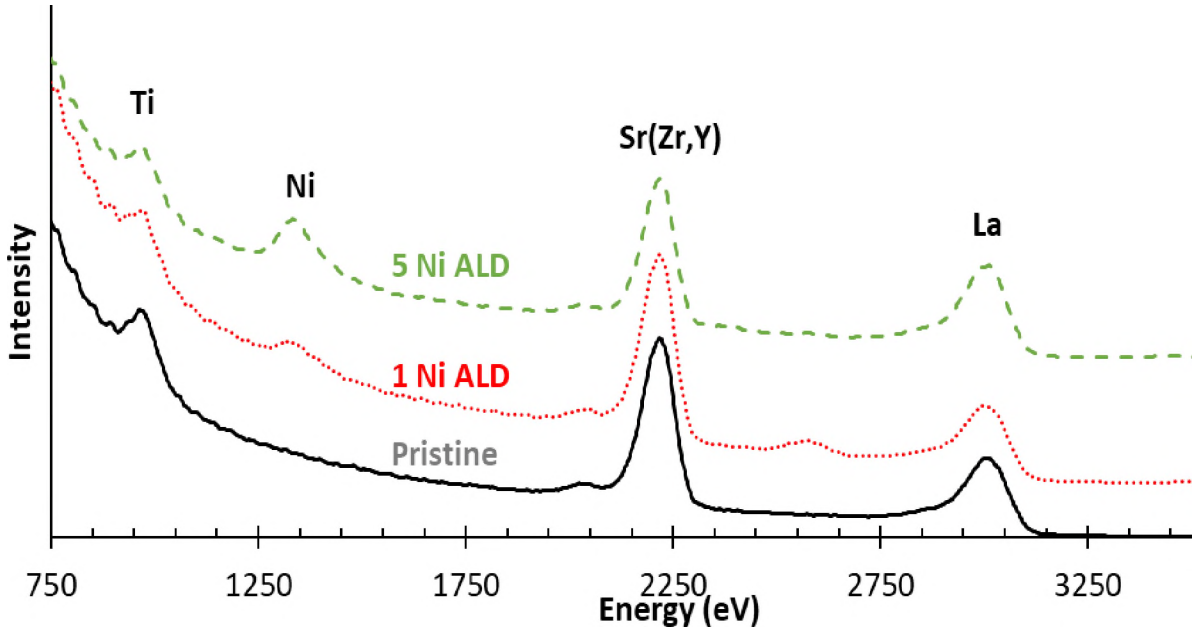

Figure 3. HS-LEIS spectra for LST-YSZ electrodes with: 0, 1, or 5 cycles of Ni ALD. The ALD spectra are offset vertically for clarity.

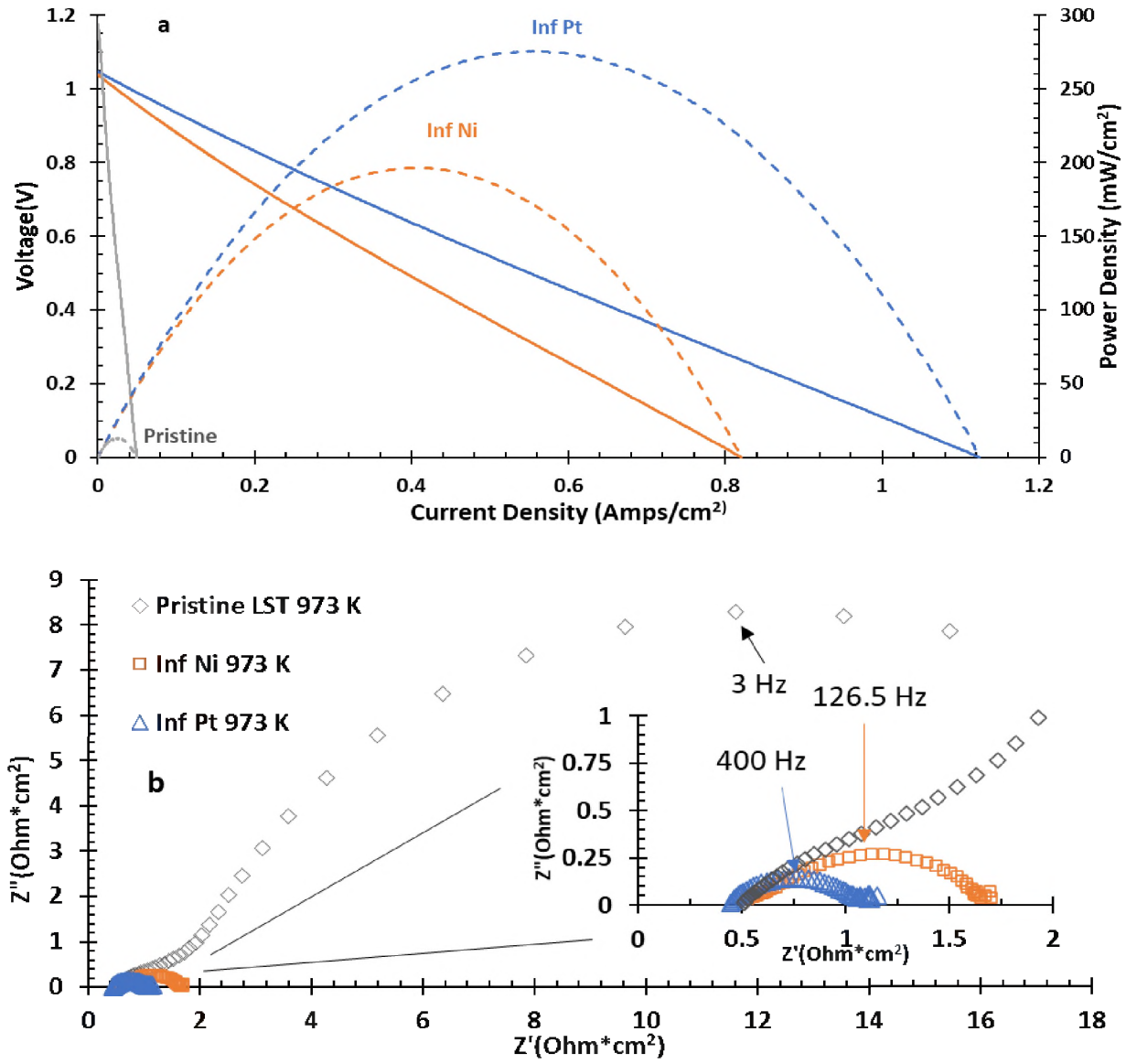

Figure 4. Performance of a pristine LST-YSZ||YSZ||LSF-YSZ cell, a cell with Ni infiltrated into the LST-YSZ, and a cell with Pt infiltrated into the LST-YSZ at 973 K: (a) IV-curves (solid) & power density curves (dashed), (b) impedance spectra.

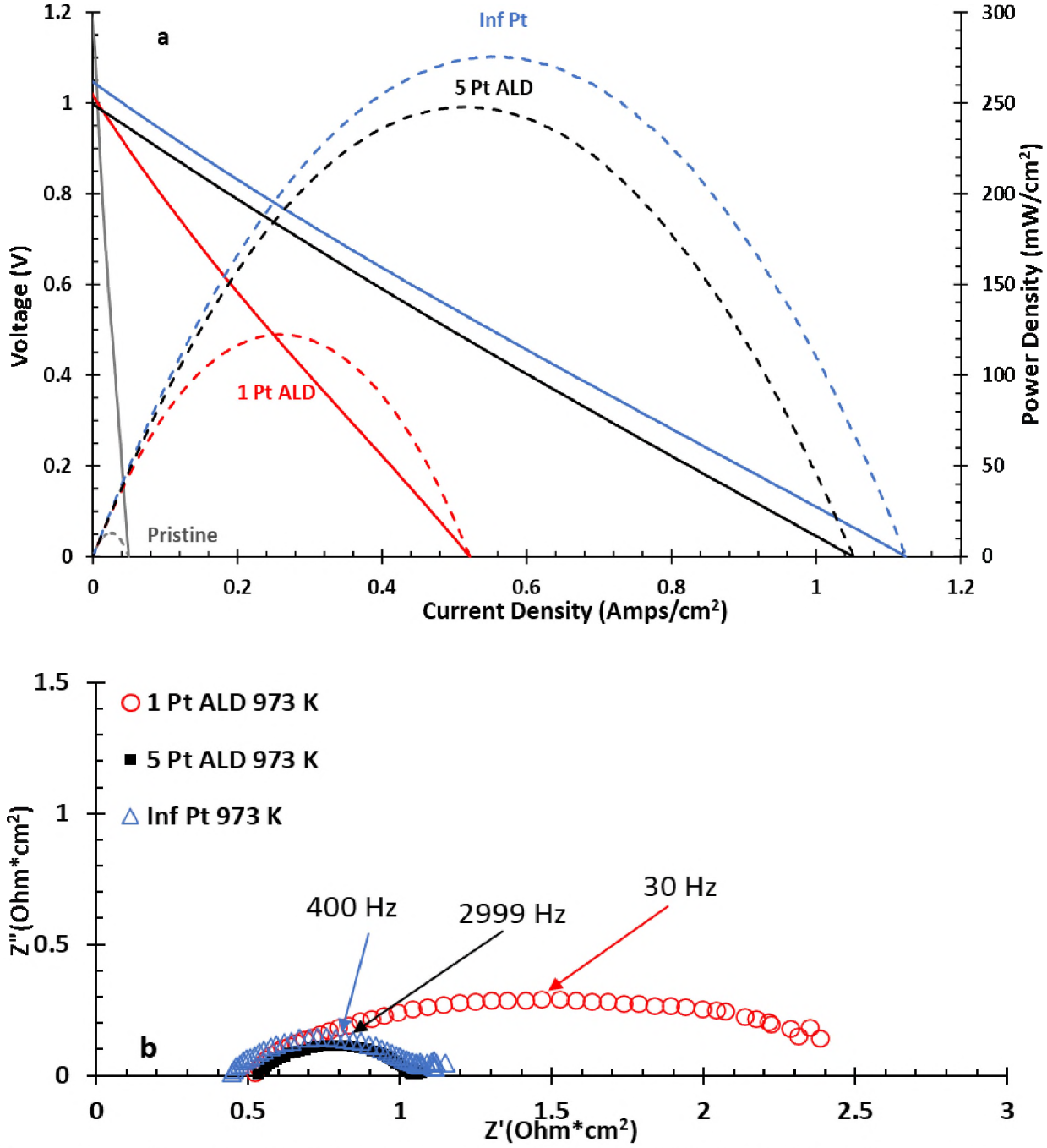

Figure 5: Performance of Pristine & Pt modified LST-YSZ||YSZ||LSF-YSZ cells at 973 K: (a) IV-curves (solid) and power density curves (dashed), (b) impedance spectra.

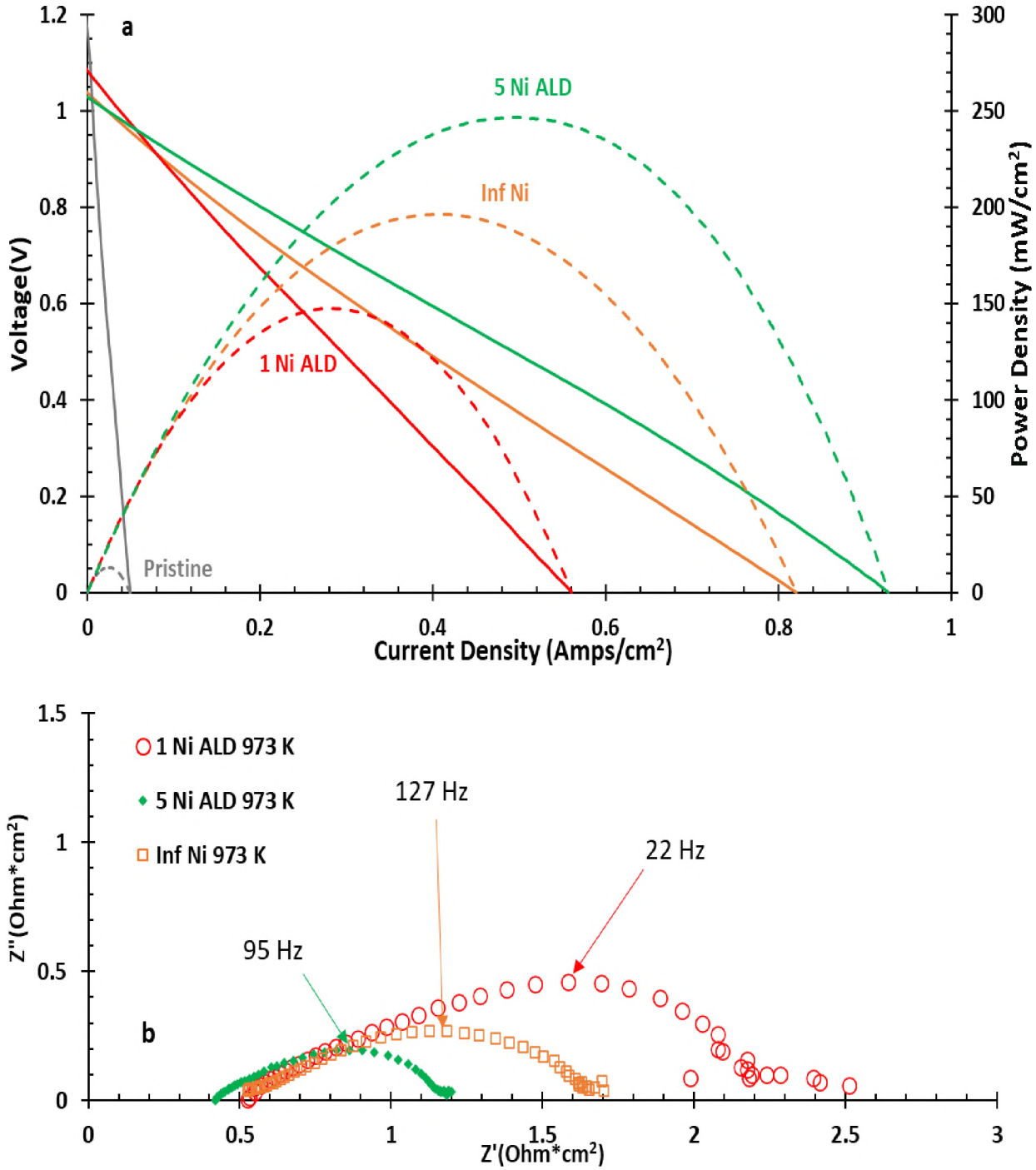

Figure 6: Performance of Pristine & Ni modified LST-YSZ||YSZ||LSF-YSZ cells at 973 K: a. IV-curves (solid) & power density curves (dashed) b. EIS spectra.

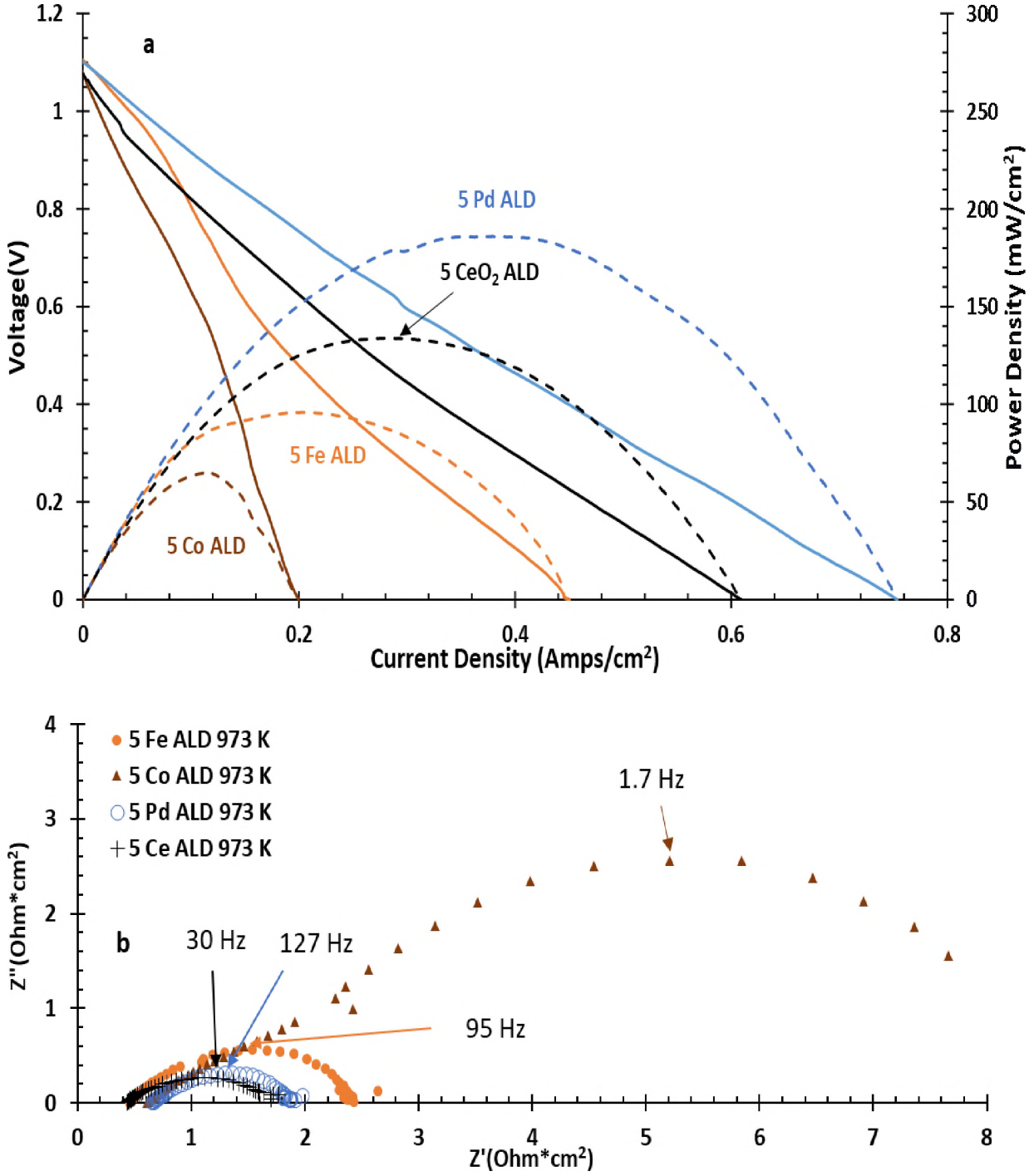

Figure 7: Performance of 5 Fe ALD, 5 Co ALD, 5 Ce ALD, and 5 Pd ALD cells at 973 K: (a) IV-curves (solid) and power density curves (dashed), (b) impedance spectra.

References

1. M.B. Mogensen, M. Chen, H.L. Frandsen, C. Graves, J.B. Hansen, K. V. Hansen, A. Hauch, T. Jacobsen, S.H. Jensen, T.L. Skafte, X. Sun, *Clean Energy*, **3**, 175–201 (2019).

2. M. Ettler, G. Blaß, and N. H. Menzler, *Fuel Cells*, **7**, 349–355 (2007).

3. T. Klemensø and M. Mogensen, *J. Am. Ceram. Soc.*, **90**, 3582–3588 (2007).

4. K. Sasaki, K. Haga, T. Yoshizumi, D. Minematsu, E. Yuki, R. Liu, C. Uryu, T. Oshima, T Ogura, Y. Shiratori, K. Ito, M. Koyama, K. Yokomoto, *J. Power Sources*, **196**, 9130–9140 (2011) http://dx.doi.org/10.1016/j.jpowsour.2010.09.122.

5. L. Yang, Z. Cheng, M. Liu, and L. Wilson, *Energy Environ. Sci.*, **3**, 1804–1809 (2010).

6. W. Wang, C. Su, Y. Wu, R. Ran, and Z. Shao, *Chem. Rev.*, **113**, 8104–8151 (2013).

7. J. Xiao, Y. Xie, J. Liu, and M. Liu, *J. Power Sources*, **268**, 508–516 (2014) http://dx.doi.org/10.1016/j.jpowsour.2014.06.082.

8. A. Atkinson, S. Barnett, R.J. Gorte, J.T.S. Irvine, A.J. McEvoy, M. Mogensen, S.C. Singhal, J. Vohs, *Nat. Mater.*, **3**, 17–27 (2004).

9. S. Primdahl, J. R. Hansen, L. Grahl-Madsen, and P. H. Larsen, *J. Electrochem. Soc.*, **148**, A74 (2001).

10. N. Danilovic, A. Vincent, J-L. Luo, K.T. Chuang, R. Hui, A.R. Sanger, Chem. Mater., 22, 957–965 (2010).

11. G. Pudmich, B.A. Boukamp, M. Gonzalez-Cuenca, W. Jungen, W. Zipprich, F. Tietz, *Solid*

State Ionics, **135**, 433–438 (2000).

12. L. Adijanto, V. Balaji Padmanabhan, K. J. Holmes, R. J. Gorte, and J. M. Vohs, *J. Solid State Chem.*, **190**, 12–17 (2012) http://dx.doi.org/10.1016/j.jssc.2012.01.065.

13. L. Adijanto, R. Küngas, J. Park, J. M. Vohs, and R. J. Gorte, *Int. J. Hydrogen Energy*, **36**, 15722–15730 (2011).

14. A. Rothschild, W. Menesklou, H. L. Tuller, and E. Ivers-Tiffée, *Chem. Mater.*, **18**, 3651–3659 (2006).

15. G. Kim, M. D. Gross, W. Wang, J. M. Vohs, and R. J. Gorte, **155**, 360–366 (2008).

16. S. Lee, G. Kim, J. M. Vohs, and R. J. Gorte, *J. Electrochem. Soc.*, **155**, B1179–B1183 (2008).

17. G. Kim, G. Corre, J. T. S. Irvine, J. M. Vohs, and R. J. Gorte, *Electrochem. Solid-State Lett.*, **11**, 16–19 (2008).

18. G. Kim, S. Lee, J. Y. Shin, G. Corre, J. T. S. Irvine, J. M. Vohs, and R. J. Gorte, Electrochem. Solid-State Lett., 12, 48–52 (2009).

19. J. S. Kim, V. V. Nair, J. M. Vohs, and R. J. Gorte, *Scr. Mater.*, **65**, 90–95 (2011).

20. J. S. Park, I.D Hasson, M.D. Gross, C. Chen, J.M. Vohs, R.J. Gorte, J. Power Sources, 196, 7488–7494 (2011) http://dx.doi.org/10.1016/j.jpowsour.2011.05.028.

21. P. M. Mortensen and I. Dybkjær, *Appl. Catal. A Gen.*, **495**, 141–151 (2015) http://dx.doi.org/10.1016/j.apcata.2015.02.022.

22. S. Tao and J. T. S. Irvine, *Chem. Rec.*, **4**, 83–95 (2004).

23. B. A. Rosen, *Electrochem*, **1**, 32–43 (2020).

24. D. Neagu, T.S. Oh, D.N. Miller, H. Ménard, S.M. Bukhari, S.R. Gamble, R.J. Gorte, J.M. Vohs, J.T.S. Irvine, *Nat. Commun.*, **6** (2015).

25. K.J. Kim, H. Han, T. Defferriere, D. Yoon, S. Na, S.J. Kim, A.M. Dayaghi, J. Son, T.S. Oh, H.M. Jang, G.M. Choi, J. Am. Chem. Soc., 141, 7509–7517 (2019).

26. J. H. Park, J-H. Lee, K. J. Yoon, H. Kim, H-I. Ji, S Yang, S Park, S. M. Han, J-W. Son, *Acta Mater.*, **206** (2021).

27. A. Pandiyan, V. D. Palma, V. Kyriakou, W. M. M. Kessels, M. Creatore, M. C. M. van de Sanden, M. N. Tsampas, *ACS Sustain. Chem. Eng.*, **8**, 12646–12654 (2020).

28. W. Wang, M. D. Gross, J. M. Vohs, and R. J. Gorte, *J. Electrochem. Soc.*, **154**, B439 (2007).

29. Y. Cheng, T.-S. Oh, R. Wilson, R. J. Gorte, and J. M. Vohs, *J. Electrochem. Soc.*, **164**, F525–F529 (2017).

30. J. M. Paige, Y. Cheng, P.A. Pepin, C.D. Curran, D. Sun, M.U. Chen, S. McIntosh, J.M. Vohs, R.J. Gorte, *Solid State Ionics*, **341** (2019).

31. T. M. Onn, R. Küngas, P. Fornasiero, K. Huang, and R. J. Gorte, *Inorganics*, **6** (2018).

32. X. Mao, A. Foucher, E. A. Stach, and R. J. Gorte, *Catal. Letters*, **149**, 905–915 (2019) http://dx.doi.org/10.1007/s10562-019-02699-6.

33. X. Mao, A. C. Foucher, E. A. Stach, and R. J. Gorte, *Inorganics*, **7**, 1–12 (2019).

34. C. Lin, A.C. Foucher, Y. Ji, C. D. Curran, E. A. Stach, S. McIntosh, and R. J. Gorte, *ACS Catal.*, **9**, 7318–7327 (2019).

35. J. W. Fergus, *J. Power Sources*, **162**, 30–40 (2006).

36. S.-I. Lee, J. M. Vohs, and R. J. Gorte, *J. Electrochem. Soc.*, **151**, A1319 (2004).

37. X. Mao, A. C. Foucher, T. Montini, E. A. Stach, P. Fornasiero, and R.J. Gorte, *J. Am. Chem. Soc.*, **142**, 10373–10382 (2020).

38. Z. H. Bi and J. H. Zhu, *J. Electrochem. Soc.*, **158**, B605 (2011).

39. C. Carrillo, T. R. Johns, H. Xiong, A. DeLaRiva, S. R. Challa, R. S. Goeke, K. Aryushkova, W. Li, C. H. Kim, A. K. Datye, J. Phys. Chem. Lett., 5, 2089–2093 (2014).

40. J. Jones, H. Xiong, A. T. DeLaRiva, E. J. Peterson, H. Pham, S. R. Challa, G. Qi, S. Oh, M. H. Wiebenga, X. I. Pereira Hernández, Y. Wang, A. K. Datye, Science (80-.)., 353, 150–154 (2016).

41. C. W. Tanner, K. Fung, and A. V. Virkar, *J. Electrochem. Soc.*, **144**, 21–30 (1997).

42. X. Song, A. R. Diaz, A. Benard, and J. D. Nicholas, *Struct. Multidiscip. Optim.*, **47**, 453–464 (2013).